RSC Advances

PAPER

View Article Online
View Journal | View Issue

Cite this: *RSC Adv.*, 2026, **16**, 2384

Thermally stable network-structured polysiloxane hybrimers with high refractive index for optical applications

Kyungkuk Koh, Seongjin Kim and Honglae Sohn *

In this study, network-structured polysiloxane hybrimers (NPH 1–3) were synthesized for high-performance optical encapsulation, focusing on advanced LED applications. Among them, NPH 3 exhibited exceptional optical and mechanical properties. At wavelengths of 450, 520, and 635 nm, it demonstrated a high refractive index of 1.61, 1.59, and 1.58, respectively, and an outstanding transmittance of 96.5% at 450 nm. The material exhibited rapid curing within 4.5 hours and a high hardness of 76.2 Shore D, surpassing conventional encapsulants like epoxy resins and commercial silicone polymers. Notably, NPH 3 maintained excellent thermal stability, as thermal aging at 200 °C for 72 h resulted in only a marginal decrease in transmittance from 96.5% to 96%, which demonstrates its remarkable resistance to optical degradation under prolonged high temperature exposure. This high thermal resilience, together with its superior refractive properties, boosts light extraction efficiency by minimizing internal reflections, rendering the material exceptionally attractive for various optoelectronic applications. Beyond traditional LED encapsulation, the impressive thermal stability expands its applicability to systems operating at elevated temperatures, such as high power LED systems, high resolution sensors, photonic devices, aerospace and automotive electronics, and high-temperature industrial sensors. NPH 3 exhibits a well balanced set of properties, including high optical transparency, rapid curing kinetics, and enhanced mechanical strength, attributed to its network-structured phenylsiloxane framework. These characteristics collectively identify NPH 3 as a promising candidate for next-generation encapsulant materials in advanced optoelectronic systems where long-term reliability and high operational efficiency are essential.

Received 23rd September 2025
Accepted 30th December 2025

DOI: 10.1039/d5ra07228j

rsc.li/rsc-advances

1 Introduction

Light-emitting diodes (LEDs) have become ubiquitous in lighting, displays, and automotive systems due to their superior energy efficiency and extended operational lifetimes. However, a critical limitation in LED performance persists due to optical losses arising from refractive index mismatch at the encapsulant–semiconductor interface, where total internal reflection can trap up to approximately 70% of the generated light, severely compromising light extraction efficiency (LEE).[1] To address this challenge, high-refractive index polymers with exceptional optical transparency and thermal stability have been increasingly developed and employed across advanced optical applications including OLEDs, high-performance CMOS image sensors, and CCD microlenses, enabling substantial improvements in photon extraction efficiency, device longevity, and operational durability. In particular, the encapsulation layer in LED systems serves as a critical protective barrier against mechanical damage, thermal cycling, and moisture ingress, demanding both superior optical clarity and sustained thermal stability during prolonged operation. Given that LED light extraction efficiency is fundamentally dependent on the encapsulant's refractive index and optical transmittance, sophisticated molecular engineering of polymeric systems is imperative to meet commercial requirements and achieve optimal device performance.[2,3]

Conventional silicone-based polymeric encapsulants typically exhibit refractive index in the range of 1.50–1.60, which result in substantial optical losses due to total internal reflection at the semiconductor interface (n = 2.50–3.50). Some carbon-based polymers containing heavy atom such as S, P, and Se exhibit refractive index in the range of 1.6–1.7.[4] Notably, within the refractive index window of 1.30–1.70, the light extraction efficiency (LEE) improves nonlinearly with increasing encapsulant refractive index, whereas beyond a refractive index of approximately 1.70, the LEE reaches almost 100%.[5,6] Consequently, the development of high-refractive index polymers with refractive index exceeding 1.60 is of paramount importance for minimizing optical confinement and effectively enhancing overall device performance. A rational molecular design strategy involves the incorporation of substituents characterized by low

Department of Chemistry, Chosun University, Gwangju 61452, Korea. E-mail: hsohn@chosun.ac.kr; Tel: +82 62 230 7372

molar volumes and high molar refraction, such as halogens, sulfur-containing moieties, and rigid aromatic frameworks, into the polymer backbone to achieve the desired optical properties. These structural modifications enhance the electronic polarizability of the matrix, enabling refractive index modulation without detriment to optical transparency, thermal endurance, or mechanical integrity, thereby supporting compatibility with large-scale device fabrication.[7–9] Although commercial epoxy resins offer adequate visible light transmittance and moisture barrier properties, their intrinsic limitations, including low refractive index ($n \approx 1.50$–1.55), poor thermal resistance above 150 °C, and susceptibility to thermally induced yellowing, render them unsuitable for high-brightness LED systems requiring extended operation at elevated junction temperatures.[10–12] In contrast, silicone-based polymers offer superior thermal stability (200 °C), inherent optical clarity, and a tunable refractive index, making them attractive alternatives for demanding LED encapsulation. For example, polyphenylsiloxane (PH) exhibits a refractive index of ~1.56 at 450 nm with 90% optical transmittance and thermal stability up to 200 °C, while polysiloxane–silphenylene hybrimer (PSH) achieves values up to 1.60. Nevertheless, these systems still face a trade-off, as concurrently attaining refractive index beyond 1.60 and superior mechanical robustness remains challenging. To overcome these limitations, we developed a rational molecular design strategy employing linear siloxane oligomers (LSO) as multifunctional cross-linkers. Unlike conventional rigid cross-linkers that exhibit localized Si–H reactivity, LSO molecules feature delocalized hydrosilyl groups distributed along the oligomeric backbone, enabling omnidirectional cross-linking reactivity. This architectural approach facilitates high phenyl content incorporation while minimizing steric hindrance and maintaining network uniformity, thereby simultaneously achieving refractive index exceeding 1.60 with excellent optical transmittance and thermal stability.

2 Experimental

2.1. Materials

Dichlorodiphenylsilane ($(C_6H_5)_2SiCl_2$, 97%), dichlorodimethylsilane ($(CH_3)_2SiCl_2$, ≥99.5%), dichloromethylsilane (CH_3SiHCl_2, ≥97%), chlorodimethylsilane ($(CH_3)_2SiHCl$, 98%), barium hydroxide monohydrate ($Ba(OH)_2 \cdot H_2O$, 98%), platinum(0)-1,3-divinyl-1,1,3,3-tetramethyldisiloxane complex solution (in xylene, Pt ~2%) were purchased from Sigma-Aldrich Co., Ltd. Magnesium sulfate anhydride ($MgSO_4$, 99%), sodium bicarbonate ($NaHCO_3$, 99.5%), and organic solvents such as tetrahydrofuran (THF), toluene, diethyl ether and *n*-hexane, methanol, acetone were purchased from OCI Co., Ltd. All organic solvents were distilled from sodium/benzophenone under argon gas. Vinyltrimethoxysilane ($(CH_3O)_3SiCHCH_2$, 97%), dichlorophenylsilane($C_6H_5SiHCl_2$) were purchased from Gelest, Inc.

2.2. Instrumentation

Optical properties were evaluated by measuring the transmittance with a UV-vis spectrophotometer (UV-2401 PC, Shimadzu, Kyoto, Japan) and the wavelength-dependent refractive index with a spectroscopic ellipsometer (M2000, Woollam, Lincoln, USA). Mechanical hardness was assessed using a Shore durometer (GS-702N, Teclock, Nagano, Japan). Structural characterization was conducted through ^1H and ^{13}C NMR spectroscopy (Bruker AC-300 MHz) and Fourier-transform infrared (FT-IR) spectroscopy (Nicolet 5700, Thermo Scientific, Waltham, USA) equipped with a diffuse reflectance attachment (Spectra-Tech). Thermal stability was analyzed by thermogravimetric analysis (TGA) using a TGA-50H instrument (Shimadzu, Kyoto, Japan) under nitrogen atmosphere at a heating rate of 10 °C min^{-1}.

2.3. Synthesis of diphenylsilanediol (DPSD)

DPSD was prepared according to a method described previously.[12] In a 2 L round-bottom flask, sodium bicarbonate (6.52 g, 78.7 mmol) was completely dissolved in 800 mL of distilled water. The solution was then cooled to 0 °C using an ice bath. While maintaining the temperature at 0 °C, dichlorodiphenylsilane (10 g, 39.5 mmol) was added dropwise with constant stirring. Upon completion of the addition, the reaction mixture was stirred for an additional 1 hour at 0 °C. The resulting white solid was extracted with diethyl ether (200 mL), and the resulting organic layer was washed repeatedly with distilled water and brine to remove residual salts. The organic layer was dried over anhydrous $MgSO_4$, filtered, and concentrated under reduced pressure. The product was subsequently recrystallized from toluene to afford diphenylsilanediol (DPSD) as a white crystalline solid (6.75 g, 31.2 mmol) in 80% yield. ^1H NMR (300 MHz, $CDCl_3$) δ 7.74–7.68 (m, 4H), 7.48–7.36 (m, 6H), 2.78 (m, 2H); ^{13}C NMR (75 MHz, $CDCl_3$) δ 134.5, 130.8, 128.2.

2.4. Synthesis of phenyl-vinyl-oligosiloxane (PVO)

PVO was prepared according to a method described previously.[13] In a 100 mL round-bottom flask equipped with a reflux condenser, diphenylsilanediol (DPSD, 10 g, 46.2 mmol), vinyltrimethoxysilane (VTMS, 4.57 g, 30.8 mmol), and $Ba(OH)_2H_2O$ (0.026 g, 0.1 mmol) were combined. The reaction mixture was heated under reflux at 80 °C with stirring for 24 hours. Upon completion of the reaction, the mixture was concentrated under reduced pressure to remove methanol by product. Subsequently, the catalyst was removed by filtration through a Teflon membrane filter (pore size: 0.30 μm). The resulting product was isolated as a colorless viscous oil.

2.5. Synthesis of linear siloxane oligomer 1 (LSO 1)

In a 250 mL round-bottom flask, 100 mL of distilled water and 100 mL of diethyl ether were combined, and the mixture was stirred under an argon atmosphere. The reaction temperature was maintained at 0 °C using an ice bath during the simultaneous addition of dichlorophenylsilane (6.85 g, 38.7 mmol) and dichlorodimethylsilane (5.00 g, 38.7 mmol), and the mixture was stirred for 10 min. Chlorodimethylsilane (2.33 g, 20.3 mmol) was added slowly at 0 °C, and the mixture was stirred for 30 min. The ice bath was removed, and stirring was continued at room temperature for 2 h. After completion of the reaction,

the organic layer was separated and washed with distilled water to remove residual HCl. The organic phase was then dried over anhydrous $MgSO_4$ and filtered. Diethyl ether was removed under reduced pressure, and the resulting solution was filtered through a G4 glass filter to afford LSO 1 as a colorless viscous oil. ^{1}H-NMR (300 MHz, $CDCl_3$) δ 7.85–7.18 (m, 20H), 5.43–4.57 (m, 6H), 0.38–0.01 (m, 36H).

2.6. Synthesis of linear siloxane oligomer 2 (LSO 2)

In a 250 mL round-bottom flask, 100 mL of distilled water and 100 mL of diethyl ether were combined, and the mixture was stirred under an argon atmosphere. The reaction temperature was maintained at 0 °C using an ice bath during the simultaneous addition of dichlorophenylsilane (5.13 g, 28.9 mmol) and dichlorodimethylsilane (7.48 g, 57.9 mmol), and the mixture was stirred for 10 min. Chlorodimethylsilane (2.33 g, 20.3 mmol) was added slowly at 0 °C, and the mixture was stirred for 60 min. The ice bath was removed, and stirring was continued at room temperature for 2 h. After completion of the reaction, the organic layer was separated and washed with distilled water to remove residual HCl. The organic phase was then dried over anhydrous $MgSO_4$ and filtered. Diethyl ether was removed under reduced pressure, and the resulting solution was filtered through a G4 glass filter to afford LSO 2 as a colorless viscous oil. ^{1}H-NMR (300 MHz, $CDCl_3$) δ 7.81–7.19 (m, 15H), 5.40–4.61 (m, 5H), 0.5–0.01 (m, 48H).

2.7. Synthesis of linear siloxane oligomer 3 (LSO 3)

In a 250 mL round-bottom flask, 100 mL of distilled water and 100 mL of diethyl ether were combined, and the mixture was stirred under an argon atmosphere. The reaction temperature was maintained at 0 °C using an ice bath during the simultaneous addition of dichlorophenylsilane (15.41 g, 87.0 mmol) and dichlorodimethylsilane (4.99 g, 38.7 mmol), and the mixture was stirred for 10 min. Chlorodimethylsilane (2.33 g, 20.3 mmol) was added slowly at 0 °C, and the mixture was stirred for 90 min. The ice bath was removed, and stirring was continued at room temperature for 2 h. After completion of the reaction, the organic layer was separated and washed with distilled water to remove residual HCl. The organic phase was then dried over anhydrous $MgSO_4$ and filtered. Diethyl ether was removed under reduced pressure, and the resulting solution was filtered through a G4 glass filter to afford LSO 3 as a colorless viscous oil. ^{1}H-NMR (300 MHz, $CDCl_3$) δ 7.88–7.05 (m, 45H), 5.42–4.60 (m, 11H), 0.39–0.01 (m, 36H).

2.8. Synthesis of NPH 1

PVO (2.00 g; 5.3 mmol with respect to the $Si(CH{=}CH_2)(-OSiPh_2)_{3/2}$ repeat units) was mixed with LSO 1 (0.7 g, 0.90 mmol) under nitrogen until homogeneous. 0.1 wt% of Pt Karstedt's catalyst in xylene (~2% of Pt) was added, and the mixture was stirred at room temperature for 2 h. Volatile components were removed under reduced pressure, and the formulation was cast into glass molds pretreated with hexaphenylcyclotrisiloxane (HPTS) as a release agent. The specimens were thermally cured in air at 180 °C and demolded to afford NPH 1 as transparent films.

2.9. Synthesis of NPH 2

PVO (2.00 g; 5.3 mmol) was mixed with LSO 2 (0.84 g, 1.06 mmol) under nitrogen until homogeneous. 0.1 wt% of Pt Karstedt's catalyst in xylene (~2% of Pt) was added, and the mixture was stirred at room temperature for 2 h. Volatile components were removed under reduced pressure, and the formulation was cast into glass molds pretreated with hexaphenylcyclotrisiloxane (HPTS) as a release agent. The specimens were thermally cured in air at 180 °C and demolded to afford NPH 2 as transparent films.

2.10. Synthesis of NPH 3

PVO (2.00 g; 5.3 mmol) was mixed with LSO 3 (0.63 g, 0.48 mmol) under nitrogen until homogeneous. 0.1 wt% of Pt Karstedt's catalyst in xylene (~2% of Pt) was added, and the mixture was stirred at room temperature for 2 h. Volatile components were removed under reduced pressure, and the formulation was cast into glass molds pretreated with hexaphenylcyclotrisiloxane (HPTS) as a release agent. The specimens were thermally cured in air at 180 °C and demolded to afford NPH 3 as transparent films.

3 Results and discussion

3.1. Silicone-based cross-linkers

Recently, several silicone-based cross-linkers for the synthesis of polysiloxane-based hybrimers have been developed and shown in Fig. 1. The PH system, utilizing PTDMSS as a cross-linker, exhibits spatially asymmetric Si–H group localization, thereby constraining hydrosilylation reaction kinetics and diminishing reactivity uniformity. This non-uniform cross-linking network results in localized density fluctuations within the encapsulant matrix, leading to spatial variations in refractive index that cause light scattering and haze formation, thereby reducing optical transparency and light transmittance.[14] These incompletely reacted, spatially hindered Si–H groups give rise to residual unreacted species that are susceptible to thermal and photochemical decomposition under prolonged LED operation, thereby accelerating yellowing and

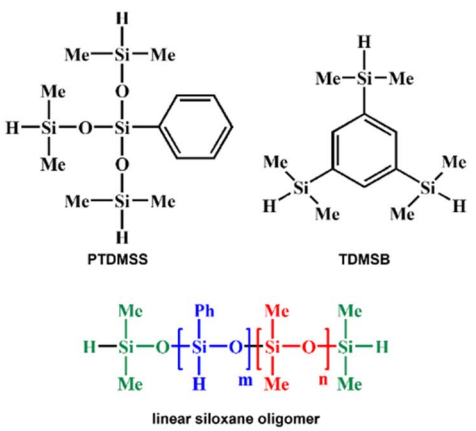

Fig. 1 Representative cross-linker units employed in the fabrication of polysiloxane hybrimers: PTDMSS,[13] TDMSB,[21] and LSO (this work).

discoloration and ultimately degrading the long-term optical reliability and color stability of the package, as previously reported in the literature.[15] PSH system was architected to employ TDMSB as a cross-linker, thereby promoting omnidirectional and uniform hydrosilyl reactivity. While this design strategy successfully achieves favorable optical characteristics, including high optical transmittance, the inherent structural limitations of the PSH formulation constrain the refractive index to approximately 1.60, which falls short of the elevated refractive index values required for optimized light extraction efficiency in advanced LED encapsulation applications.[16] To overcome the limitations inherent in conventional polysiloxane-based hybrimers, this study was designed to develop an advanced encapsulant material by strategically incorporating multiple Si–H functional sites within linear siloxane oligomer (LSO) cross-linkers.

This molecular architecture enables omnidirectional and uniform hydrosilylation reactivity while simultaneously circumventing steric hindrance effects through the inherent linear structural configuration. Furthermore, the deliberate introduction of multiple Si–Ph functional groups into the LSO framework facilitates the achievement of refractive index exceeding 1.60, while maintaining robust thermal stability at elevated temperatures. The resulting network-structured polysiloxane hybrimer (NPH) materials demonstrate a synergistic combination of superior optical performance, exceptional mechanical properties, and outstanding thermal reliability, thereby establishing a comprehensive solution for next-generation high-performance LED encapsulation applications.

3.2. Characterization of NPH 1–3

The synthetic pathway for phenyl-vinyl-oligosiloxane (PVO) is illustrated in Scheme 1A, which involves a sol–gel condensation reaction between methoxysilanes and silanol groups. Specifically, the methoxy (–OCH_3) groups of vinyltrimethoxysilane (VTMS) undergo nucleophilic substitution with the silanol (Si–OH) groups of diphenylsilanediol (DPSD) *via* deprotonation of hydroxyl groups, leading to the formation of covalently bonded siloxane (Si–O–Si) linkages.[13,14,16–21] To suppress the cleavage of phenyl groups typically observed under acidic conditions, barium hydroxide was selected as a mild basic catalyst to promote siloxane condensation. A nonhydrolytic sol–gel strategy was employed to avoid the introduction of water, which is known to reduce resin stability by inducing hydrolytic side reactions. Under these anhydrous conditions, silane monomers underwent direct condensation *via* nucleophilic substitution, leading to the formation of siloxane oligomers with enhanced structural integrity.[16,21,22] The resulting phenyl-vinyl-oligosiloxane (PVO) was obtained as a colorless, viscous oil and its molecular structure was confirmed by ^{1}H and ^{13}C nuclear magnetic resonance (NMR) spectroscopy, which verified the complete incorporation of phenyl and vinyl functionalities without detectable hydrolysis by products (Scheme 1A).[14] Linear siloxane oligomer cross-linkers (LSO 1–3) with Si–Ph contents of 30%, 50%, and 70% were systematically designed and employed as cross-linking units. Linear siloxane oligomer cross-linkers LSO 1–3 were synthesized in a biphasic H_2O/diethyl ether medium by varying the dichlorophenylsilane : dichlorodimethylsilane feed ratio and quenching with chlorodimethylsilane (Scheme 1B). As shown in Scheme 1C, the NPH 1–3 was synthesized *via* a platinum-catalyzed hydrosilylation reaction between sol–gel derived phenyl-vinyl-oligosiloxane (PVO) and linear siloxane oligomers (LSO 1–3), employed as multifunctional linear cross-linking agents. In this study, the molar ratio of vinyl groups in phenyl-vinyl-oligosiloxane (PVO) to hydrosilyl groups in linear siloxane oligomers (LSO 1–3) was

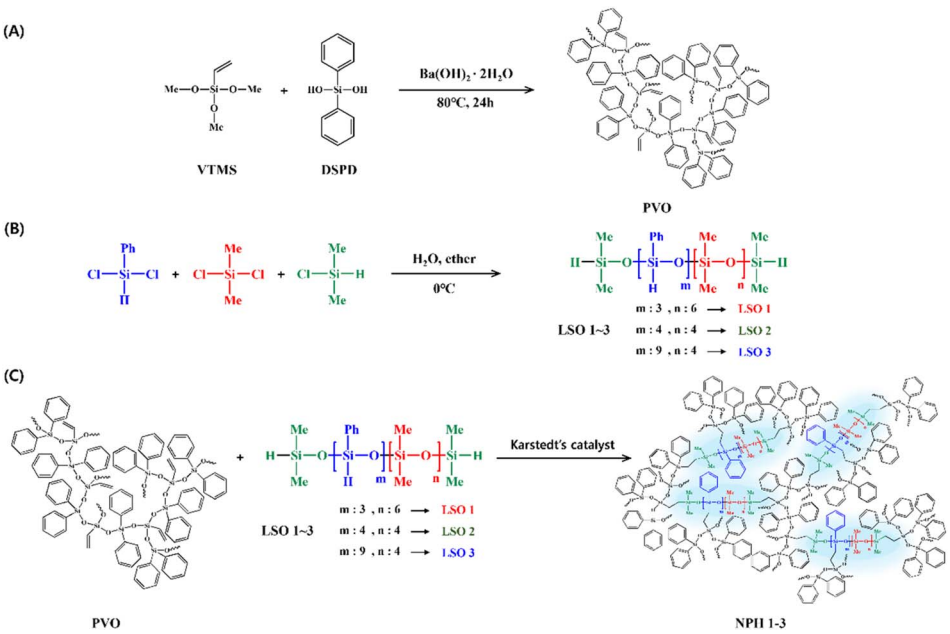

Scheme 1 Synthesis of (A) phenyl-vinyl-oligosiloxane (PVO), (B) linear siloxane oligomers cross-linker (LSO 1–3 cross-linker) and (C) the network-structured polysiloxane hybrimer 1–3 (NPH 1–3) by the hydrosilylation of PVO and LSO 1–3.

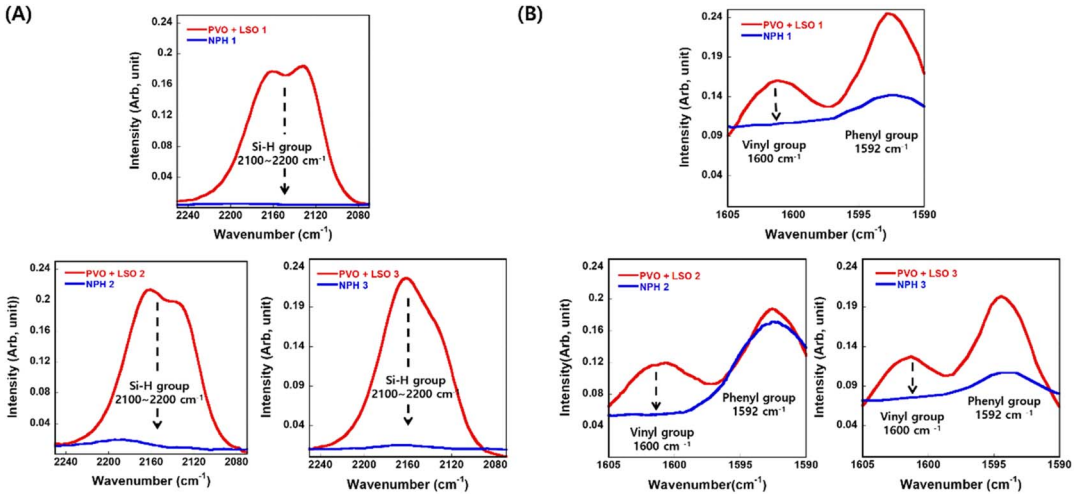

Fig. 2 FT-IR spectra of (A) Si–H stretching vibrations (2100–2200 cm^{-1}) and (B) vinyl group C=C stretching vibration (~1600 cm^{-1}) before and after thermal curing of the network-structured polysiloxane hybrimers (NPH 1–3).

optimized to 1 : 1. Karstedt's catalyst loading was adjusted to 0.1 wt% relative to the total weight of the PVO and LSO 1–3 mixture, and hydrosilylation reactions were conducted at 180 °C under ambient atmospheric conditions. For each composition, curing experiments were conducted at least three times, and three specimens were prepared for each Si–Ph fraction. Each specimen was analyzed by FT-IR spectroscopy to monitor the decrease in Si–H and C=C absorption peaks after curing. To evaluate the relationship between curing time and hardness, ten specimens were prepared and cured at 30 min intervals from 0 to 5 hours. The hardness of each specimen was measured three times, and the averaged values were used for analysis. All other experiments, including thermogravimetric analysis (TGA), optical transmittance measurements, and thermal aging tests, were also performed at least three times to ensure reproducibility.

3.3. FT-IR analysis of NPH 1–3

The FT-IR spectra of the uncured resin exhibited a characteristic absorption band at 2120 cm^{-1}, corresponding to the Si–H stretching vibration of the hydrosilane moieties in LSO 1–3 and another band at 1600 cm^{-1}, attributed to the C=C stretching vibration of the vinyl groups in the PVO matrix.

Upon thermal curing at 180 °C in the presence of a platinum catalyst, the FT-IR spectra of NPH 1–3 (Fig. 2) showed the complete disappearance of the Si–H (~2120 cm^{-1}) and C=C (~1600 cm^{-1}) bands, indicating quantitative consumption of the reactive functionalities. This spectral change provides direct evidence that hydrosilylation proceeded to completion, wherein vinyl and hydrosilane groups were covalently cross-linked to generate a 3D siloxane network. Consistent with these observations, the curing reaction reached completion within 4.5 h under the specified conditions. The observed morphological and spectroscopic data suggest that the optimized formulation successfully minimizes structural heterogeneity within the polymer network. The 1 : 1 molar ratio between vinyl and hydrosilyl groups, combined with controlled reaction kinetics and adequate pre-gel fluidity, enabled uniform distribution of cross-linking sites throughout the matrix. This uniformity effectively suppressed the formation of network imperfections such as microphase-separated clusters and dangling chain segments, which are typically associated with incomplete or uneven cross-linking. These results underscore the importance of precise stoichiometric balance and rheological control in achieving a structurally uniform and densely crosslinked network, as inferred from spectroscopic, thermal, mechanical, and optical measurements, which is essential for enhancing the mechanical and optical performance of the resulting hybrid material. Among the samples, the formulation based on LSO 3 exhibited the lowest residual Si–H and vinyl vibrational intensities in the FT-IR spectra.

3.4. Curing behavior and hardness properties

The thermal curing behavior of the network-structured polysiloxane hybrimers (NPH 1–3) was systematically investigated by monitoring Shore D hardness development at 180 °C, as presented in Fig. 3A. The hardness evolution profiles exhibited distinct differences across the three formulations, with NPH 3 demonstrating the most favorable curing characteristics. Specifically, NPH 3 achieved a Shore D hardness of 70 within 2.5 h and exhibited continuous hardness development, reaching 76.2 Shore D after 4.5 h of thermal curing. The progressive hardness increase observed for NPH 3 can be attributed to the structural characteristics of the long-chain linear cross-linker, which incorporates multiple Si–H reactive sites. This molecular design effectively moderates the curing rate during the initial stages while sustaining steady cross-linking conversion throughout the latter stages of the curing process. The attainment of high terminal hardness (76.2 Shore D) serves as direct evidence for the formation of a densely cross-linked network and substantiates the suitability of NPH 3 for LED encapsulation, providing effective mechanical protection for the semiconductor chip, enhanced package stability, and improved gas-barrier properties.

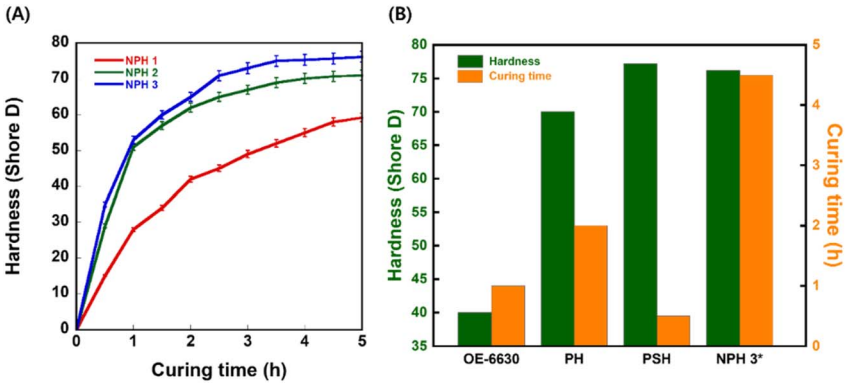

Fig. 3 (A) Shore D hardness evolution of NPH 1–3 during curing at 180 °C. Hardness values at 2.5 h and 4.5 h were as follows: NPH 1 (65 and 71 Shore D), NPH 2 (45 and 59 Shore D), and NPH 3 (70 and 76.2 Shore D). (B) hardness (Shore D) and curing time of various polysiloxane-based materials, including OE-6630,[9] PH,[13] PSH,[21] and NPH 3.

As shown in Fig. 3B, the comparative analysis of hardness properties for silicone-based encapsulant systems reveals that the NPH 1–3 exhibit mechanical performance comparable to or superior to previously reported PH and PSH, while delivering markedly enhanced hardness relative to the commercial encapsulant OE-6630 (Dow Corning, Shore D = 40).[10] In particular, NPH 3 achieved a Shore D hardness of 76.2, corresponding to an approximately 1.8 times improvement over OE-6630. This result indicates that, unlike conventional siloxane-based cross-linkers, the LSO employed in NPH 3, which contains multiple Si–H reactive sites, enables efficient high-density crosslinking with PVO. Although this molecular design leads to a somewhat slower curing rate, it ultimately affords a robust and rigid hybrid network. The superior mechanical hardness of NPH 3 is attributed to the high phenyl-group content incorporated within the LSO cross-linker, which promotes the development of a more rigid molecular architecture throughout the NPH matrix.

This clear structure property relationship establishes a direct correlation between increased phenyl content and enhanced mechanical rigidity, positioning NPH 3 as an optimal candidate for high-performance LED encapsulation applications.

3.5. Thermal stability properties

Thermal stability of NPH 1–3 was systematically assessed by thermogravimetric analysis (TGA), as presented in Fig. 4A and B. Full-range measurements (0–700 °C) revealed comparable mass loss values across all samples at elevated temperatures, with NPH 1 exhibiting 32.9% mass loss, NPH 2 showing 31.8% loss, and NPH 3 demonstrating 31.3% loss. Furthermore, thermal stability was evaluated based on $T_{d5\%}$ (the temperature at which 5% mass loss occurs), a common indicator of the onset of thermal decomposition in polymers. Excellent thermal performance was confirmed across all samples, with NPH 1 exhibiting a $T_{d5\%}$ of 324 °C, NPH 2 of 331 °C, and NPH 3 of 342 °C. Within the practical LED encapsulant operating temperature range (150–200 °C), as shown in Fig. 4B, significant differentiation in low-temperature thermal stability was observed. At 150 °C, NPH 1 exhibited 0.8% mass loss, NPH 2 showed 0% loss, and NPH 3 remained stable with 0% loss. At 200 °C, mass loss values were NPH 1 (1.2%), NPH 2 (0.1%), and NPH 3 (0%), respectively. The superior low-temperature thermal stability of NPH 3 is attributed to the robust cross-linked network architecture formed through platinum-catalyzed hydrosilylation between PVO and LSO 3 (silphenyl : dimethylsilyl molar ratio = 9 : 4), combined with the

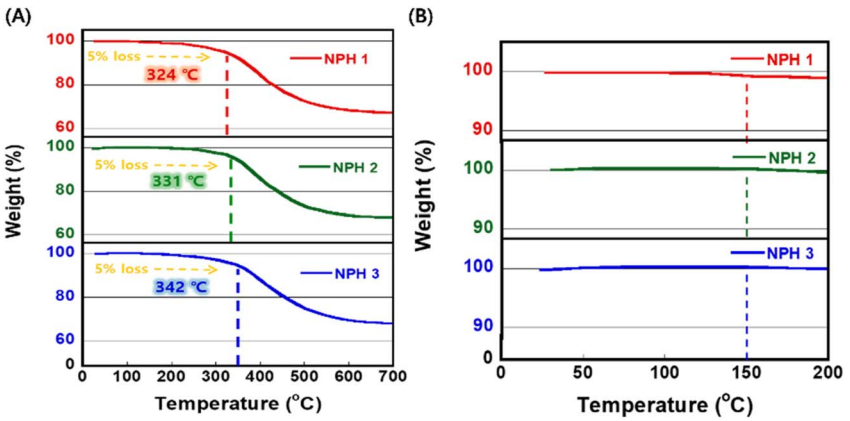

Fig. 4 TGA curves of NPH 1–3. (A) Displays the overall thermogravimetric analysis curves of NPH 1–3 from 0 °C to 700 °C, while (B) highlights the structural stability of NPH 1–3 between 0 °C and 200 °C. NPH 1 exhibited negligible weight loss (0.8% at 150 °C and 1.2% at 200 °C), NPH 2 showed modest weight loss (0% at 150 °C; 0.1% at 200 °C), and NPH 3 displayed no measurable weight loss at either temperature.

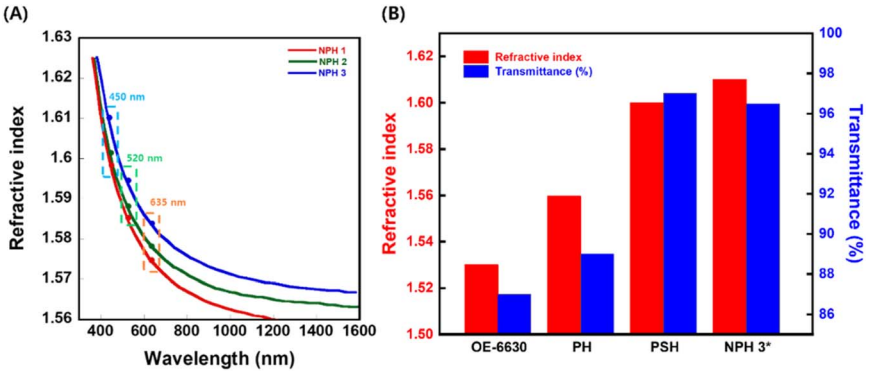

Fig. 5 (A) Refractive index (n) of NPH 1–3 at 450, 520, and 635 nm: NPH 1 exhibits $n = 1.59$, 1.58, and 1.57; NPH 2 displays $n = 1.60$, 1.58, and 1.57; NPH 3 demonstrates $n = 1.61$, 1.59, and 1.58 across the respective wavelengths. (B) Refractive index and transmittance at 450 nm for OE-6630 (Dow Corning),[9] PH,[13] PSH,[21] and NPH 3 (* indicates this work).

elevated Si–Ph content incorporated within the cross-linker, which collectively enhance thermal resistance.

3.6. Optical properties

3.6.1. Refractive index and transmittance properties. The refractive index of NPH 1–3 specimens were systematically determined using spectroscopic ellipsometry (M2000, J.A. Woollam, Lincoln, USA), with results summarized in Fig. 5A. Notably, NPH 3, which incorporates the highest Si–Ph functional group content and the longest linear chain structure, achieved the highest refractive index values of 1.61, 1.59, and 1.58 at 450, 520, and 635 nm, respectively. NPH 2, containing an intermediate number of Si–Ph functional groups, exhibited refractive index of 1.60, 1.58, and 1.57 at the respective wavelengths. In contrast, NPH 1, which incorporates the lowest Si–Ph functional group content, demonstrated refractive index of 1.59, 1.58, and 1.57 at 450, 520, and 635 nm, respectively.

These experimental findings definitively establish a direct and systematic relationship between the Si–Ph functional group content incorporated within the LSO cross-linker and the experimentally measured refractive index values, thereby corroborating the structure property correlations previously documented in the literature.[23,24] Fig. 5B presents a comparative analysis of refractive index and optical transmittance at 450 nm for a series of polysiloxane-based materials, including PH, PSH, NPH, and the commercial encapsulant OE-6630 (Dow Corning). Among the evaluated systems, NPH demonstrated superior overall optical performance, achieving a refractive index of 1.61 and optical transmittance of 96.5% at 450 nm. In comparison, the PH system exhibited a refractive index of 1.56 with optical transmittance of 89% at 450 nm, while the PSH system achieved a refractive index of 1.60 with notably higher transmittance of 97% at 450 nm, as confirmed by both experimental measurements and literature reports.[14,21] Among the siloxane-based hybrimers evaluated, NPH 3 demonstrated the highest refractive index value of 1.61, representing a significant advancement in optical performance.

To gauge the practical significance of this refractive-index enhancement, we estimated the change in light-extraction efficiency at a GaN ($n \approx 2.5$)/encapsulant interface using a simple escape-cone model. Increasing the encapsulant index from 1.60, representative of PSH-type polysiloxane hybrimers, to 1.61 for NPH 3 enlarges the critical angle from ~39.8° to ~40.1°, which increases the fraction of photons that can escape into the encapsulant from ≈23.2% to ≈23.5%. This corresponds to a relative gain of ~1.4% in interface light-extraction efficiency. Although this improvement appears modest in absolute numerical terms, such percentage-level enhancements are technologically relevant in high-brightness LED packages and are achieved here without sacrificing optical transmittance and while providing substantially improved thermal and mechanical stability compared with conventional polysiloxane hybrimers. Consequently, NPH 3 is expected to afford a measurable increase in luminous flux as well as improved lumen maintenance under long-term high-temperature operation.

3.6.2. Thermal optical properties. Comparative optical transmittance measurements across the wavelength range of 350–700 nm were performed for the synthesized NPH series and the commercial encapsulant OE-6630 (Dow Corning),[25] with all specimens prepared at a standardized thickness of 2 mm (Fig. 6A). At 450 nm, the commercial standard OE-6630 exhibited a transmittance of 87%, while the NPH series demonstrated transmittance values of 59%, 95%, and 96.5% for NPH 1, NPH 2, and NPH 3, respectively. Notably, both NPH 2 and NPH 3 achieved transmittance values that exceed the optical performance of the commercialized OE-6630 standard, with NPH 3 demonstrating the highest transmittance of 96.5% among all evaluated materials. In contrast, NPH 1 exhibited the lowest transmittance at 59%, which reflects the limited optical clarity resulting from inadequate cross-linking density and network homogeneity in this particular formulation. Among the NPH series, NPH 3 exhibited excellent optical transparency and demonstrated strong resistance to heat-induced yellowing under thermal aging conditions at 200 °C in air, indicating that optical degradation is effectively suppressed even under harsh thermal environments. Optical stability was quantitatively assessed by recording UV-vis transmittance spectra of NPH 1–3 and the commercial encapsulant OE-6630 (Dow Corning) across the wavelength range of 350–700 nm before and after thermal aging at 200 °C for 72 h (Fig. 6A–E). NPH 3 demonstrated exceptional thermal stability,

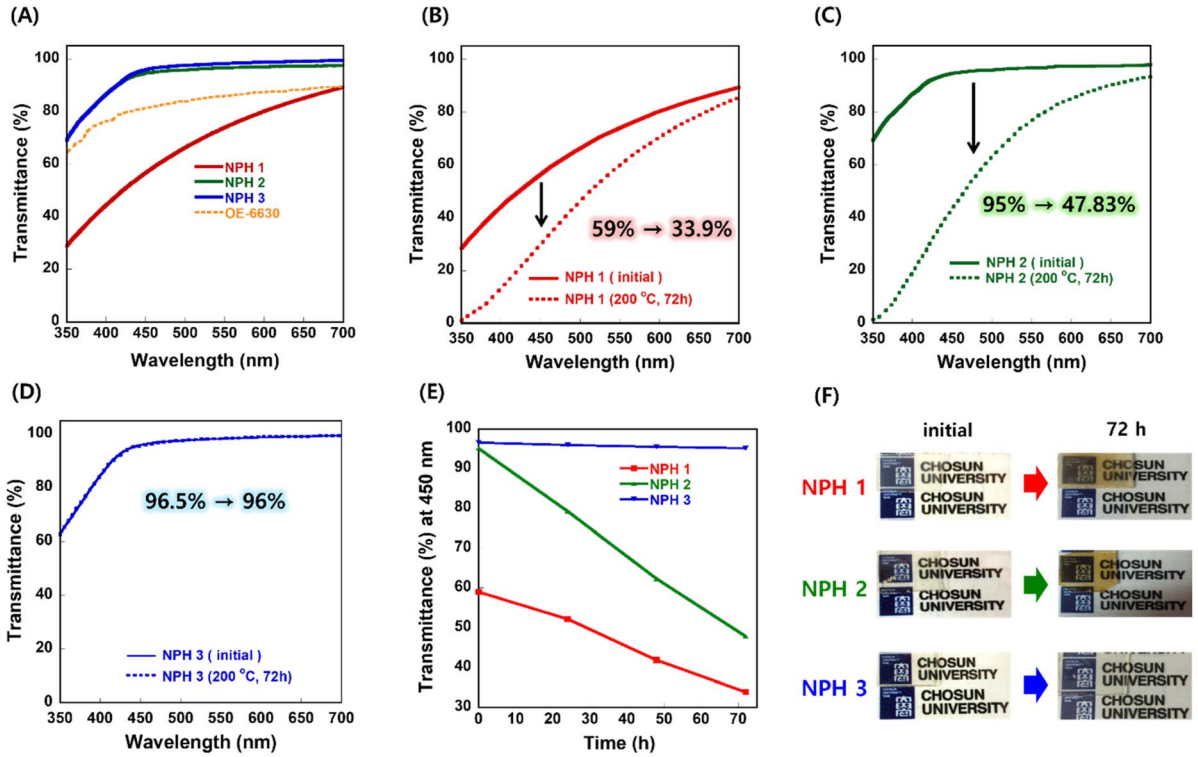

Fig. 6 UV-vis transmittance spectra (350–700 nm) of NPH 1–3 and the commercial encapsulant OE-6630 (Dow Corning, dotted orange line) with a thickness of 2 mm (A). NPH 1 (350–700 nm) exhibited a significant decrease at 450 nm from 59% to 33.9% following thermal aging at 200 °C for 72 h (B). NPH 2 (350–700 nm) exhibited a significant decrease at 450 nm from 95% to 47.83% following thermal aging at 200 °C for 72 h (C). NPH 3 (350–700 nm) exhibited a significant decrease at 450 nm from 96.5% to 96% following thermal aging at 200 °C for 72 h (D). Time-dependent UV-vis transmittance of NPH 1–3 at 450 nm during thermal aging at 200 °C (E). Photographs of NPH 1–3 samples before and after thermal aging at 200 °C for 72 h (F).

maintaining a high initial transmittance of 96.5% at 450 nm (Fig. 6A), which decreased only marginally to 96% following thermal treatment, representing a minimal loss of 0.5%. In contrast, NPH 1 exhibited significantly lower thermal durability, with an initial transmittance of only 59% at 450 nm, which underwent substantial degradation upon thermal aging, declining to 33.9% and resulting in a transmittance reduction of 25.1% (Fig. 6B). NPH 2 demonstrated good initial optical performance with transmittance of 95% at 450 nm; however, its thermal stability proved inadequate, as the transmittance severely decreased to 47.83% after thermal aging at 200 °C for 72 h, corresponding to a reduction of 47.17% (Fig. 6C). The transmittance degradation profiles presented in Fig. 6E clearly illustrate the superior thermal stability of NPH 3 compared to NPH 1 and NPH 2 across the extended thermal aging period. Photographic comparisons of the samples before and after thermal aging further substantiated these quantitative findings (Fig. 6F). NPH 1 and NPH 2 displayed visible yellowing and discoloration following thermal treatment, while NPH 3 maintained its optical clarity and transparency without any observable discoloration, thereby confirming its superior resistance to thermally induced degradation. The markedly enhanced thermal stability of NPH 3 is attributed to its molecular structure, which incorporates a long-chain linear siloxane oligomer (LSO) crosslinker with multiple Si–H reactive sites and a high proportion of phenyl-substituted silicon (Si–Ph) functional groups. These structural features collectively promote the formation of a highly homogeneous and densely cross-linked network, effectively suppressing the formation of degradation prone residual reactive species and structural defects. These comprehensive results establish NPH 3 as a promising candidate for high-performance LED encapsulation applications, offering substantially improved thermal durability and long-term optical reliability under elevated temperature conditions.

4 Conclusions

In this work, a series of network-structured polysiloxane hybrimers (NPH 1–3) were successfully synthesized *via* the hydrosilylation of phenyl-vinyl-oligosiloxane (PVO) with linear siloxane oligomers (LSO 1–3). This strategy enables 1 : 1 stoichiometric optimization and an omnidirectional distribution of hydrosilyl groups, resulting in structurally uniform and densely crosslinked network, as inferred from spectroscopic, thermal, mechanical, and optical measurements. Among the prepared materials, NPH 3 exhibited the most favorable optical performance, with a refractive index of 1.61 and an optical transmittance of 96.5% at 450 nm, surpassing previously reported polysiloxane hybrimers (PH, $n = 1.56$; PSH, $n = 1.60$). Under accelerated thermal aging at 200 °C for 72 h, NPH 3 retained excellent optical stability, showing only a 0.5% decrease in transmittance (from 96.5% to 96.0%), while also maintaining

robust mechanical properties (Shore D = 76.2) and fast curing behavior (4.5 h). The well-balanced combination of high optical transparency, mechanical rigidity, and thermal durability highlights NPH 3 as a promising encapsulant for next-generation LED devices and suggests its potential for broader application in high-temperature optoelectronic systems.

Author contributions

Conceptualization, H. S.; methodology, K. K.; investigation, K. K.; data curation, K. K., S. K.; formal analysis, K. K., S. K.; writing – original draft preparation, K. K.; writing – review and editing, H. S.; supervision, H. S.; project administration, H. S.; funding acquisition, H. S. All authors have read and approved the final version of the manuscript.

Conflicts of interest

The authors declare no competing financial interest.

Data availability

The data that support the findings of this study are available from the corresponding author upon reasonable request.

Acknowledgements

This work was supported by the Technology Innovation Program (or Industrial Strategic technology development program, RS-2022-00154968) and the Regional Innovation System & Education (RISE) program through the (Gwangju RISE Center), funded by the Ministry of Education (MOE) and the (Gwangju Metropolitan City), Republic of Korea (2025-RISE-05-013). This study was supported by a research fund from Chosun University, 2026.

References

1 E. F. Schubert and J. K. Kim, *Science*, 2005, **308**, 1274–1278.
2 J. Zhang, T. Bai, W. Liu, M. Li, Q. Zang, C. Ye, J. Z. Sun, Y. Shi, J. Ling, A. Qin and B. Z. Tang, *Nat. Commun.*, 2023, **14**, 3524.
3 S. Watanabe and K. Oyaizu, *Bull. Chem. Soc. Jpn.*, 2023, **96**, 1108–1128.
4 D. Ryu, M. Lee, H. Sohn and N. Yoo, *Macromol. Res.*, 2023, **31**, 583–592.
5 M. Ma, F. W. Mont, X. Yan, J. Cho, E. F. Schubert, G. B. Kim and C. Sone, *Opt. Express*, 2010, **49**, 12–20.
6 D. Sikdar, J. B. Pendry and A. A. Kornyshev, *Light:Sci. Appl.*, 2020, **09**, 122.
7 K. Mazumder, B. Voit and S. Banerjee, *ACS Omega*, 2024, **9**, 6253–6279.
8 S. Iino, S. Sobu, K. Nakabayashi, S. Samitsu and H. Mori, *Polymer*, 2021, **224**, 123725.
9 Y. H. Kim, J.-Y. Bae, J. Jin and B.-S. Bae, *ACS Appl. Mater. Interfaces*, 2014, **6**, 3115–3121.
10 H. Kim, J.-Y. Bae, Y. H. Kim, Y. B. Kim and B.-S. Bae, *J. Appl. Polym. Sci.*, 2013, **131**, 39968.
11 W.-F. Su, Y.-C. Fu and W.-P. Pan, *Thermochim. Acta*, 2002, **392–393**, 385–389.
12 C.-W. Hsu, C.-C. M. Ma, C.-S. Tan, H.-T. Li, S.-C. Huang, T.-M. Lee and H. Tai, *Mater. Chem. Phys.*, 2012, **134**, 789–796.
13 M. Luo and B. Yan, *Tetrahedron Lett.*, 2009, **50**, 5208–5209.
14 J.-S. Kim, S. Yang and B.-S. Bae, *Chem. Mater.*, 2010, **22**, 3549–3555.
15 J. Shen and Y. Feng, *Silicon*, 2023, **15**, 2163–2172.
16 J.-Y. Bae, Y. H. Kim, H.-Y. Kim, Y.-W. Lim and B.-S. Bae, *RSC Adv.*, 2013, **3**, 8871–8877.
17 A. A. Issa and A. S. Luyt, *Polymers*, 2019, **11**, 537.
18 R. J. Hofmann, M. Vlatković and F. Wiesbrock, *Polymers*, 2017, **9**, 534.
19 S. Jana, M. A. Lim, I. C. Baek and S. I. Seok, *Mater. Chem. Phys.*, 2008, **112**, 1008–1014.
20 K. Krupiński, J. Wagler, E. Brendler and E. Kroke, *Gels*, 2023, **9**, 291.
21 K. Koh and H. Sohn, *Polymers*, 2021, **13**, 515.
22 Y. Lu, Z. Zhao, X. Fan, X. Cao, M. Hai, Z. Yang, K. Zheng, J. Lu, J. Zhang, Y. Ma, R. Zhang and S. Fang, *RSC Adv.*, 2021, **11**, 18326–18332.
23 X. Hao, J. L. Jeffery, T. P. T. Le, G. McFarland, G. Johnson, R. J. Mulder, Q. Garrett, F. Manns, D. Nankivil, E. Arrieta, A. Ho, J.-M. Parel and T. C. Hughes, *Biomaterials*, 2012, **33**, 5659–5671.
24 X. X. Shang, S. Duan, M. Zhang, X. Y. Cao, K. Zheng, J. N. Zhang, Y. M. Ma and R. B. Zhang, *RSC Adv.*, 2018, **8**, 9049–9056.
25 Y. H. Kim, Y.-W. Lim, D. Lee, Y. H. Kim and B.-S. Bae, *J. Mater. Chem. C*, 2016, **4**, 10791–10796.